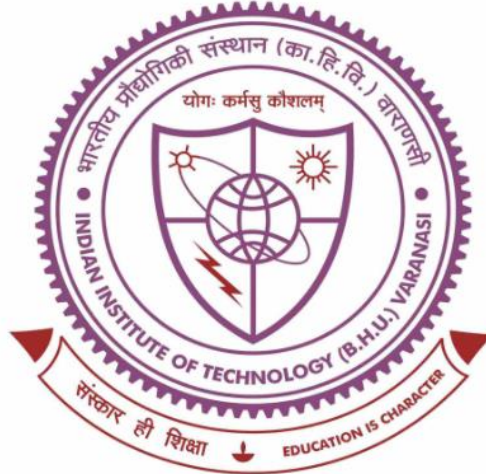


Development of Bi-Based Lead-Free Piezoelectric Ceramics for High Temperature Applications



THESIS SUBMITTED IN PARTIAL FULFILLMENT

FOR THE AWARD OF DEGREE

DOCTOR OF PHILOSOPHY

By

Srishti Paliwal

School of Materials Science and Technology
Indian Institute of Technology
(Banaras Hindu University)
Varanasi - 221005, India

Roll No: 19111005

2024

"The important thing is not to stop questioning. Curiosity has its own reason for existing".

ALBERT EINSTEIN

DEDICATED TO.....

MY LOVING FAMILY

& FRIENDS



भारतीय
प्रौद्योगिकी
संस्थान
काशी हिन्दू विश्वविद्यालय



INDIAN
INSTITUTE OF
TECHNOLOGY
BANARAS HINDU UNIVERSITY

CERTIFICATE

It is certified that the work contained in the thesis titled **“Development of Bi-Based Lead-Free Piezoelectric Ceramics for High Temperature Applications”** by **“Srishti Paliwal”** has been carried out under my supervision and that this work has not been submitted elsewhere for a degree.

It is further certified that the student has fulfilled all the requirements of Comprehensive Examination, Candidacy and SOTA for the award of Ph.D. Degree.

Date: 29/June/2024
Place: Varanasi

Signature:

(Dr. Akhilesh Kumar Singh)
Supervisor

(Professor & Coordinator)
School of Materials Science & Technology,
IIT(BHU), Varanasi-221005

Professor/आचार्य
School of Materials Science & Technology/पदार्थ विज्ञान एवं प्रौद्योगिकी स्कूल
Indian Institute of Technology/भारतीय प्रौद्योगिकी संस्थान
(Banaras Hindu University), Varanasi/काशी हिन्दू विश्वविद्यालय, वाराणसी



भारतीय
प्रौद्योगिकी
संस्थान
काशी हिन्दू विश्वविद्यालय



INDIAN
INSTITUTE OF
TECHNOLOGY
BANARAS HINDU UNIVERSITY

DECLARATION OF THE CANDIDATE

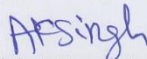
I, Srishti Paliwal, certify that the work embodied in this Ph.D. thesis is my own bonafide work and carried out by me under the supervision of Professor Akhilesh Kumar Singh for a period from July 2019 to June 2024 at the School of Materials Science and Technology, Indian Institute of Technology, (BHU), Varanasi. The matter embodied in this thesis has not been submitted for the award of any other degree/diploma. I declare that I have faithfully acknowledged and given credits to the research workers wherever their works have been cited in my work in this thesis. I further declare that I have not wilfully copied any other's work, paragraphs, text, data, results, etc. reported in the journals, books, magazines, reports, dissertations, thesis, etc., or available at websites and included them in this Ph.D. thesis and have not cited as my own work.

Date: 29/June/2024
Place: Varanasi

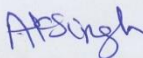

(Srishti Paliwal)

CERTIFICATE BY THE SUPERVISOR

This is to certify that the above statement made by the candidate is correct to the best of my knowledge.


(Dr. Akhilesh Kumar Singh)
Supervisor
(Professor & Coordinator)
School of Materials Science & Technology,
IIT(BHU), Varanasi-221005

Professor/आचार्य
School of Materials Science & Technology/पदार्थ विज्ञान एवं प्रौद्योगिकी स्कूल
Indian Institute of Technology/भारतीय प्रौद्योगिकी संस्थान
(Banaras Hindu University), Varanasi/काशी हिन्दू विश्वविद्यालय, वाराणसी


Coordinator of the School
Coordinator/समन्वयक
School of Materials Science & Technology/पदार्थ विज्ञान एवं प्रौद्योगिकी स्कूल
Indian Institute of Technology/भारतीय प्रौद्योगिकी संस्थान
(Banaras Hindu University), Varanasi/काशी हिन्दू विश्वविद्यालय, वाराणसी

COPYRIGHT TRANSFER CERTIFICATE

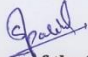
Title of the Thesis: "Development of Bi-Based Lead-Free Piezoelectric Ceramics for High Temperature Applications"

Name of the Student: Srishti Paliwal

Copyright Transfer

The undersigned hereby assigns to the Indian Institute of Technology (Banaras Hindu University) all rights under copyright that may exist in and for the above thesis submitted for the award of the "Doctor of Philosophy".

Date: 21/June/2024
Place: Varanasi


Signature of the Student
(Srishti Paliwal)

Note: However, the author may reproduce or authorize others to reproduce materials extracted verbatim from the thesis or derivative of the thesis for author's personal use provided that the source and the Institute's copyright notices are indicated.

Acknowledgements

Firstly, I extend my deepest gratitude to my esteemed supervisor, Professor Akhilesh Kumar Singh, for his invaluable guidance, insightful suggestions, and unwavering encouragement throughout my Ph.D. journey. His faith in my ability to work independently and his support in selecting research problems aligned with my interests have significantly boosted my confidence as a researcher. His enthusiasm, patience, and kindness have been pivotal during challenging times.

I am sincerely thankful to the faculty members of the School of Materials Science and Technology, including Prof. Dhananjai Pandey, Prof. Rajiv Prakash, Prof. Pralay Maiti, Prof. Chandana Rath, Dr. Chandan Upadhyay, Dr. Bholanath Pal, Dr. Ashish Kumar Mishra, Dr. Shrawan Kumar Mishra, Dr. Sanjay Singh, Dr. Nikhil Kumar, Dr. Ravi, and Dr. Udayshankar, for their invaluable suggestions and support. Special thanks to Prof. Rajeev Kumar Singh, Department of Electrical Engineering, IIT (BHU), for his encouragement and support as an external RPEC member.

I acknowledge the Central Instrument Facility (CIF) at IIT (BHU) for providing access to essential experimental facilities.

I am deeply grateful to my labmates, Dr. Vijeyta Pal, Dr. Monika Singh, Dr. Pragyan Prajapati, Dr. Krishna Prajapati, Dr. Vishwa Pratap Singh, Mr. Ankit Dwivedi, Ms. Pooja Sonkar, Mr. Satyendra Kumar Satyarthi, Ms. Deep Mala, Mr. Prosun Mondal, and Ms. Sadhana Yadav, for their unwavering cooperation and camaraderie.

My heartfelt thanks go to my friends and colleagues, Ms. Sudepta Bauri, Ms. Swikriti Tripathi, Mr. Sudarshan Sarkar, Mr. Ravi Singh, Mr. Akhilesh Yadav, Mr. Rohit Jha and Mr. Amit Bar for their moral support and suggestions.

I owe a profound debt of gratitude to my beloved parents (Mrs. Mukta Paliwal and Mr. Rajesh Paliwal), my grandparents (Late Shri Haribhau Paliwal, Smt. Sushila Devi, Late Shri Maheshanand Kala and Smt. Raji Dev), my siblings (Mrs. Megha Paliwal, Ms. Anjali Paliwal, Mr. Aditya Paliwal) and my brother-in-law (Mr. Rakesh Dhoundiyal) for their unconditional love and support. I am extremely grateful to Mr. Sushant Batra for his patience, unwavering support, and love throughout this journey. I also appreciate Mr. Piyush Nainwal and Manisha Chauhan for their constant encouragement.

I express my appreciation to all technical and non-technical staff at IIT (BHU) for their assistance during my stay on the campus.

I acknowledge the financial assistance provided by the Government of India through the Prime Minister's Research Fellowship. I am also thankful to the Department of Science and Technology, India, and IIT (BHU) for additional financial support.

In conclusion, the journey towards my doctoral degree has been made possible by the invaluable assistance, guidance, and support of my mentors, colleagues, family, and friends. Though words may fall short, this acknowledgment is a humble attempt to express my deep appreciation to each one of you and also to all those not mentioned here.

Sincerely

Srishti Paliwal

TABLE OF CONTENTS

| | |
|---------------------------------------------------------------------------|-------------|
| Chapter 1: Introduction and Literature Review | 1-57 |
| 1.1 Motivation and General Introduction | 1 |
| 1.2 Fundamentals of Dielectrics | 4 |
| 1.2.1 Introduction to Dielectrics | 4 |
| 1.2.1.1 Mathematical Description of Polarization | 4 |
| 1.2.2 Polarization Mechanisms | 5 |
| 1.3 Basics of Piezoelectricity | 7 |
| 1.4 Overview of Ferroelectrics | 10 |
| 1.5 Overview of Relaxor Ferroelectrics | 11 |
| 1.5.1 Difference between Normal Ferroelectrics and Relaxor Ferroelectrics | 12 |
| 1.6 Perovskites | 16 |
| 1.6.1 Crystal Structure and Wyckoff Positions | 17 |
| 1.6.2 Coordination and Site Preferences | 18 |
| 1.6.3 Properties of Perovskite Oxides | 19 |
| 1.6.3.1 Electronic Properties | 20 |
| 1.6.3.2 Optical Properties | 21 |

| | |
|--------------------------------------------------------------------------------------------------------------|--------------|
| 1.6.3.3 Ionic Conductivity | 22 |
| 1.7 Transition to Lead-Free Piezoelectric Materials: Enhancing Sustainability and Mitigating Health Risks | 23 |
| 1.8 Foundational Perspective on Phase Boundaries | 25 |
| 1.8.1 Morphotropic Phase Diagram (MPB) | 25 |
| 1.8.2 Phase Boundaries in Lead-Based and Lead-Free Piezoelectric Perovskite Materials | 27 |
| 1.9 Recent Development in Bi-based Lead-free Bulk Piezoceramics | 30 |
| 1.9.1 BiFeO ₃ (BFO) Based Piezoceramics | 33 |
| 1.9.1.1 Evolution and Recent Development of BiFeO ₃ - BaTiO ₃ (BF-BT) System | 35 |
| 1.9.2 Bi _{1/2} Na _{1/2} TiO ₃ (BNT) Based Ceramics | 48 |
| 1.9.3 Bi ₄ Ti ₃ O ₁₂ (BIT) Based Piezoceramics | 49 |
| 1.10 Objective of Present Work | 55 |
| Chapter 2: Experimentation and Characterization Techniques | 58-83 |
| 2.1 Introduction | 58 |
| 2.2 Methodology for Synthesis of Samples | 59 |
| 2.2.1 Solid State Reaction Methodology | 59 |
| 2.2.2 Chemicals and Compositions | 61 |

| | |
|-------------------------------------------------------------------------------------------------------------------------------------------------------------------------------------|---------------|
| 2.3 Characterization Technique and Instrumentation | 61 |
| 2.3.1 X-ray Diffraction (XRD) Technique | 61 |
| 2.3.1.1 Basic Principle of Bragg's Law | 64 |
| 2.3.1.2 Crystal Structure Determination Using Rietveld Refinement | 65 |
| 2.3.2 Fourier Transform Infrared Spectroscopy | 66 |
| 2.3.3 Scanning Electron Microscopy (SEM) | 68 |
| 2.3.4 X-ray Photoelectron Spectroscopy (XPS) | 70 |
| 2.3.5 Dielectric Spectroscopy | 72 |
| 2.3.6 Diffuse Reflectance Ultraviolet-Visible (UV-Vis) Spectroscopy | 74 |
| 2.3.7 Ferroelectric Characterization | 75 |
| 2.3.8 Piezoelectric Charge Coefficient Measurement | 78 |
| 2.3.9 Photoluminescence Spectroscopy | 81 |
| 2.4 Conclusions | 82 |
| Chapter 3: Quenching-Driven Advancements in Functional Properties of High-Temperature Lead-Free Sc, Ga Modified 0.67BiFeO₃-0.33BaTiO₃ Relaxor Ceramics | 84-115 |
| 3.1. Introduction | 84 |
| 3.2. Experimental Procedure | 86 |
| 3.2.1. Sample preparation | 86 |

| | |
|-----------------------------------------------------------------------------------------------------------------------------------------------------------------------------------------------------------------------------------------------|----------------|
| 3.2.2. Characterizations | 89 |
| 3.3. Results and Discussions | 90 |
| 3.3.1. Structural Analysis | 90 |
| 3.3.1.1. Crystal Structure Analysis | 90 |
| 3.3.1.2. FTIR Studies | 95 |
| 3.3.1.3. XPS Studies | 98 |
| 3.3.2. Microstructural Analysis | 103 |
| 3.3.3 Electrical Characterizations | 105 |
| 3.3.3.1. Dielectric Properties | 105 |
| 3.3.3.2. Ferroelectric and Piezoelectric Properties | 109 |
| 3.4. Conclusion | 114 |
| Chapter 4: Enhanced Functionalities of Isovalently Substituted 0.67(Bi_{1-x}La_xFe_{0.97}Ga_{0.03}O₃)-0.33(BaTiO₃) Relaxor Piezoceramics Synthesized via Air Quenching | 116-142 |
| 4.1. Introduction | 116 |
| 4.2. Experimental Details and Characterization | 118 |
| 4.3. Results and Discussion | 119 |
| 4.3.1 Structural Studies | 119 |

| | |
|-----------------------------------------------------------------------------------------------------------------------------------------------------------------------------------------------------------------------------|----------------|
| 4.3.1.1 Crystal Structure Analysis | 119 |
| 4.3.1.2 FTIR Analysis | 124 |
| 4.3.1.3 X-ray Photoelectron Spectroscopy Analysis | 125 |
| 4.3.2 Microstructural Studies | 131 |
| 4.3.3 Dielectric and Ferroelectric Studies | 132 |
| 4.4 Conclusions | 142 |
| Chapter 5: Site engineering: A Tool to Enhance Functional Properties in High-Temperature Lead-Free Relaxors Prepared via Air Quenching | 143-163 |
| 5.1 Introduction | 143 |
| 5.2 Experimental Details | 145 |
| 5.3 Results and Discussion | 146 |
| 5.3.1 Crystal Structural Analysis | 146 |
| 5.3.2 Study of Optical Properties | 147 |
| 5.3.3 Dielectric Studies | 153 |
| 5.3.4 Ferroelectric Studies | 159 |
| 5.4. Conclusions | 163 |
| Chapter 6: Effect of Sintering Temperature on the Structural, Dielectric, Ferroelectric, Piezoelectric and Optical Properties of Sm/Ta Co-Doped Bi₄Ti₃O₁₂ Aurivillius Piezoceramics | 164-203 |

| | |
|---------------------------------------------------|----------------|
| 6.1 Introduction | 164 |
| 6.2 Experimental Details | 167 |
| 6.2.1 Sample Preparation | 167 |
| 6.2.2 Characterizations | 168 |
| 6.3 Results and Discussion | 169 |
| 6.3.1 Structural Analysis | 169 |
| 6.3.1.1 Crystal Structural Analysis | 169 |
| 6.3.1.2 FTIR Analysis | 172 |
| 6.3.1.3 X-ray Photoelectron Spectroscopy Analysis | 174 |
| 6.3.2 Microstructural Studies | 177 |
| 6.3.3 Ferroelectric Studies | 181 |
| 6.3.4 Dielectric and Piezoelectric Studies | 192 |
| 6.3.5 Optical Properties Studies | 198 |
| 6.4 Conclusion | 202 |
| Chapter 7: Conclusion and Future Scope | 204-209 |
| 7.1. Summary of the Thesis | 204 |
| 7.2. Future Scope | 207 |
| References | 210-233 |

| | |
|----------------------------------------------------------|------------|
| List of Publications | 234 |
| List of Conferences/Workshops/Seminars/Symposiums | 235 |

List of Figures

| Figure No. | Captions | Page No. |
|-------------|-------------------------------------------------------------------------------------------------------------------------------------------------------------------------------------------------------------------------------------------|----------|
| Figure 1.1 | Piezoelectric materials market share by 2032 (in USD Billion). | 2 |
| Figure 1.2 | Different polarization mechanisms with respect to frequency in dielectrics. | 6 |
| Figure 1.3 | Different polarization mechanisms in both presence and absence of applied electric field (a) Dipolar/Orientational/Molecular, (b) Electronic, (c) Interfacial/Space charge and (d) Ionic/ Atomic. | 7 |
| Figure 1.4 | Categorization of dielectric materials. | 8 |
| Figure 1.5 | Comprehensive comparison of normal ferroelectrics with relaxor ferroelectrics. | 14 |
| Figure 1.6 | Schematic diagram for ideal cubic perovskite structure. | 17 |
| Figure 1.7 | Key properties and applications of perovskites. | 20 |
| Figure 1.8 | (a) Phase diagram and (b) Composition dependent planar coupling coefficient and piezoelectric coefficients of $(1-x)\text{PbZrO}_3\text{-}x\text{PbTiO}_3$ solid solution. | 28 |
| Figure 1.9 | A cross-sectional analysis of the Gibbs free energy for $\text{Pb}(\text{Zr}_{1-x}\text{Ti}_x)\text{O}_3$ compositions with 90/10 and 60/40 ratios along the $[\text{M}_\text{B}]$ path. | 30 |
| Figure 1.10 | Differentiation of elements based on toxicity and cost. | 32 |
| Figure 1.11 | A broad classification of High Temperature lead-free Bi-based piezoelectric materials. | 33 |
| Figure 1.12 | (a) d_{33} vs T_C/T_m comparison for piezoelectric ceramics with max d_{33} obtained for Sn doped BT (BTS_x , $x=0.11$) (b) Temperature dependent dielectric permittivity for BTS_x with respect to Sn content. | 37 |
| Figure 1.13 | Revised phase diagram of BF-BT solid solution by (a) Leontsev et al. after Kumar et al. and (b) Kim et al. after carrying out synchrotron XRD and temperature dependent dielectric properties measurement. | 38 |

| | | |
|--------------------|-----------------------------------------------------------------------------------------------------------------------------------------------------------------------------------------------------------------------------------------------------------------------------------------------------------------------------------------------------------------------|----|
| Figure 1.14 | (a) Phase diagram of BF-BT solid solution and (b) Rhombohedral distortions ($90^\circ-\alpha_R$) and phase volume fractions of furnace-cooled BF33BT FC, water-quenched BF33BT WQ, BF33BT-3BZT, and BF33BT-3BG ceramics. | 39 |
| Figure 1.15 | (a) d_{33} and d_{33}^* values of 0.67BFO–0.33BTO (BF33BT), 0.7(BF33BT)–0.3Ba($Zr_{0.5}Ti_{0.5}$)O ₃ (BF33BT-3BZT) and 0.7(BF33BT)–0.3BiGaO ₃ BF-BT-3BG as function of BT content (b) temperature dependent dielectric constant of BF-BT ceramics (c) P-E loops of BF-BT ceramics and (d) bipolar S-E hysteresis loops of BF-BT ceramics. | 40 |
| Figure 1.16 | (a-f) P-E hysteresis loops for (1-x)BF–xBT, $0.2 \leq x \leq 0.45$, (g) variation of P_r with respect to applied electric field, and (i) d_{33} and electromechanical coupling constant k_p with respect to BT content. | 42 |
| Figure 1.17 | (a) Room temperature P-E hysteresis loops measured at 0.1 Hz and (b) Bipolar Strain-Electric field (S-E) loops for BF-BT for BF-BT ceramics with respect to BT concentration. | 43 |
| Figure 1.18 | Bright field TEM images for BF25BT samples (a) air quenched (AQ) at 800 °C and (b) furnace cooled (FC). | 47 |
| Figure 1.19 | Summary of major issues and scientific point in BF based piezoceramics. | 47 |
| Figure 1.20 | Ball stick diagram of different BLSFS. | 51 |
| Figure 1.21 | (A) SEM micrographs at different sintering temperature, (B) variation of d_{33} as a function of sintering temperature measured at RT, and (C) d_{33} as a function of annealing temperature. | 54 |
| Figure 1.22 | d_{33} vs T_c variation of different BSLFs. | 55 |
| Figure 2.1 | Pictorial representation of solid-state route adopted for preparation of samples. | 60 |
| Figure 2.2 | (a) Image of the benchtop XRD and (b) the schematic diagram showing the basic principle of Bragg's law. | 63 |
| Figure 2.3 | (a) Basic principle governing FTIR spectroscopy and (b) a typical FTIR instrument setup. | 68 |

| | | |
|--------------------|---------------------------------------------------------------------------------------------------------------------------------------------------------------------------------------------------------------------|-------|
| Figure 2.4 | (a) Schematic image of different components of SEM instrument and (b) Image of a high resolution SEM. | 70 |
| Figure 2.5 | (a) Basic principle of XPS and (b) working XPS instrument (Thermo Fisher Scientific (K-alpha)). | 72 |
| Figure 2.6 | Experimental setup to measure temperature dependent dielectric properties using Keysight impedance analyzer. | 74 |
| Figure 2.7 | (a) Basic principle and schematic picture of operation of UV-vis spectrophotometer and (b) Shimadzu UV-2600 spectrophotometer. | 75 |
| Figure 2.8 | (a) A typical P-E Hysteresis loop, (b) Schematic Sawyer Tower Circuit and (c) Ferroelectric property measurement setup by the Radiant Technologies (Precision Premier II). | 78 |
| Figure 2.9 | A typical d_{33} meter by PIEZOTEST. | 80 |
| Figure 2.10 | Fluorescence spectrophotometer (F-4600, Hitachi) for photoluminescence measurement. | 82 |
| Figure 3.1 | The schematic diagram for methodology adopted to prepare $0.67\{\text{Bi}(\text{Fe}_{0.97}\text{Ga}_{0.03})_{1-x}\text{Sc}_x\text{O}_3\}-0.33(\text{BaTiO}_3)$ ceramics, where $x=0.01$ to 0.07 . | 87 |
| Figure 3.2 | XRD patterns of $0.67\{\text{Bi}(\text{Fe}_{0.97}\text{Ga}_{0.03})_{1-x}\text{Sc}_x\text{O}_3\}-0.33(\text{BaTiO}_3)$ samples prepared using (a) CS and (b) AQ methods. | 91 |
| Figure 3.3 | Rietveld refinement fits for (a) Sc1 CS, (b) Sc1 AQ, (c) Sc3 CS, (d) Sc3 AQ, (e) Sc4 CS, (f) Sc4 AQ, (g) Sc5 CS, (h) Sc5 AQ, (i) Sc6 CS and (j) Sc6 AQ samples. | 92-93 |
| Figure 3.4 | FTIR spectra for $0.67\{\text{Bi}(\text{Fe}_{0.97}\text{Ga}_{0.03})_{1-x}\text{Sc}_x\text{O}_3\}-0.33(\text{BaTiO}_3)$ ceramics at room temperature in KBr mode prepared using (a) CS and (b) AQ sintering methods. | 96 |
| Figure 3.5 | Ball and Stick model plotted using VESTA with obtained CIF file of Sc2 CS Rietveld refinement results representing the Ti/FeO_6 octahedron and $\text{Ti}/\text{Fe}-\text{O}$ bonds. | 98 |
| Figure 3.6: | XPS spectra of (a) complete spectrum, (b) Bi 4f spectra of Sc1 CS, (c-h) O 1s for Sc1, Sc3 and Sc7 composition samples prepared using AQ and CS method. | 100 |
| Figure 3.7 | XPS spectra of Fe $2p_{3/2}$ for Sc1, Sc3, Sc5, and Sc7 samples, prepared using AQ and CS methods. | 102 |

| | | |
|--------------------|------------------------------------------------------------------------------------------------------------------------------------------------------------------------------------------------------------------------------------------------------------------------------------------------------------------------------------------------------------------------------------------------------------------------------------------------------------------------------------------------------------------------|-----|
| Figure 3.8 | SEM micrographs of $0.67\{\text{Bi}(\text{Fe}_{0.97}\text{Ga}_{0.03})_{1-x}\text{Sc}_x\text{O}_3\}-0.33(\text{BaTiO}_3)$ ceramics, both air quenched (AQ) and closed sintered (CS) samples sintered at 960°C for 2 hours (a-d) $x=0.01$, (b-e) $x=0.02$, (c-f) $x=0.03$, (g-j) $x=0.04$, (h-k) $x=0.05$, (i-l) $x=0.06$ and (m-n) $x=0.07$, along with the corresponding grain size distribution is shown in the insets; (o) average grain size variation with respect to the composition for CS and AQ samples. | 104 |
| Figure 3.9 | Comparison of temperature-dependent dielectric permittivity (ϵ_r) and loss ($\tan \delta$) at various frequencies for $0.67\{\text{Bi}(\text{Fe}_{0.97}\text{Ga}_{0.03})_{1-x}\text{Sc}_x\text{O}_3\}-0.33(\text{BaTiO}_3)$ samples prepared using AQ and CS methods. | 106 |
| Figure 3.10 | Room temperature ferroelectric polarization (P)-electric field (E) hysteresis loops at 10 Hz for (a) closed sintered (CS) samples and (b) air quenched (AQ) samples, as a function of composition. | 110 |
| Figure 3.11 | Ferroelectric polarization (P-E) hysteresis loop along with corresponding current response at 10 Hz for (a) Sc2 (b) Sc3 (c) Sc4 samples prepared by AQ method, and (d) remnant polarization (P_r) and coercive field (E_c) as a function of composition for CS and AQ samples. | 111 |
| Figure 3.12 | Current response curves for (a) Sc2 CS and Sc2 AQ, (b) Sc3 CS and Sc3 AQ, (c) Sc4 CS and Sc4 AQ. | 112 |
| Figure 3.13 | (a) Current density J (A/cm^2) and (b) Resistivity ($\text{ohm}\cdot\text{cm}$) plots with respect to composition for both AQ and CS specimens at 1 kV/cm of applied electric field. (c) comparison of piezoelectric charge coefficient, d_{33} for AQ and CS samples for different compositions. | 114 |
| Figure 4.1 | XRD patterns of $0.67(\text{Bi}_{1-x}\text{La}_x\text{Fe}_{0.97}\text{Ga}_{0.03}\text{O}_3)-0.33(\text{BaTiO}_3)$ where $x=0.01$ (La1), 0.03 (La3), 0.05 (La5), and 0.07 (La7) (a) calcined at 850 °C and (b) sintered at 980 °C for 2 hours and annealed at 550 °C for 12 hours. | 121 |
| Figure 4.2 | The Rietveld refined XRD patterns fit using cubic $\text{Pm}\bar{3}\text{m}$ space group for $0.67(\text{Bi}_{1-x}\text{La}_x\text{Fe}_{0.97}\text{Ga}_{0.03}\text{O}_3)-0.33(\text{BaTiO}_3)$ where $x=0.01$ (La1), $x=0.03$ (La3), $x=0.05$ (La5), and $x=0.07$ (La7) sintered at 980 °C for 2 hours and annealed at 550 °C for 12 hours. | 122 |

| | | |
|--------------------|------------------------------------------------------------------------------------------------------------------------------------------------------------------------------------------------------------------------------------------------------------------------------------------------------------------------------|-----|
| Figure 4.3 | Schematic ball and stick diagram of (a) perovskite unit cell (b) Fe/Ti-O ₆ octahedra in 0.67(Bi _{0.99} La _{0.01} Fe _{0.97} Ga _{0.03} O ₃)-0.33(BaTiO ₃) piezoceramics. | 123 |
| Figure 4.4 | FTIR spectra of 0.67(Bi _{1-x} La _x Fe _{0.97} Ga _{0.03} O ₃)-0.33(BaTiO ₃) where x=0.01(La1), x=0.03(La3), x=0.05(La5), and x=0.07(La7). | 125 |
| Figure 4.5 | Complete XPS spectra of (a) x=0.01(La1), and (b) x=0.03(La3) for 0.67(Bi _{1.05-x} La _x Fe _{0.97} Ga _{0.03} O ₃)-0.33(BaTiO ₃) ceramics. | 127 |
| Figure 4.6 | XPS spectra of O1s state for 0.67(Bi _{1-x} La _x Fe _{0.97} Ga _{0.03} O ₃)-0.33(BaTiO ₃) ceramics (a) x=0.01(La1), (b) x=0.03(La3), (c) x=0.05(La5), and (d) x=0.07(La7). | 128 |
| Figure 4.7 | XPS spectra of Fe2p state for 0.67(Bi _{1-x} La _x Fe _{0.97} Ga _{0.03} O ₃)-0.33(BaTiO ₃) ceramics (a) x=0.01(La1), (b) x=0.03(La3), (c) x=0.05(La5), and (d) x=0.07(La7). | 129 |
| Figure 4.8 | XPS spectra of Bi4f state for 0.67(Bi _{1-x} La _x Fe _{0.97} Ga _{0.03} O ₃)-0.33(BaTiO ₃) ceramics (a) x=0.01(La1), (b) x=0.03(La3), (c) x=0.05(La5), and (d) x=0.07(La7). | 130 |
| Figure 4.9 | SEM images and grain size distribution for (a, e) x=0.01(La1), (b, f) x=0.03(La3), (c, g) x=0.05(La5), (d, h) x=0.07(La7) and for 0.67(Bi _{1-x} La _x Fe _{0.97} Ga _{0.03} O ₃)-0.33(BaTiO ₃) samples. | 132 |
| Figure 4.10 | Temperature dependent dielectric permittivity and dielectric loss plots as a function of frequency in the range 1.26 kHz to 160 kHz for x=0.01(La1), (b) x=0.03(La3), (c) x=0.05(La5), (d) x=0.07(La7) (e) comparison of dielectric constant at 10 kHz and (f) frequency dependent dielectric constant for all compositions. | 135 |
| Figure 4.11 | Modified Curie-Weiss law plots for characterization of diffuseness parameter γ at 10 kHz for 0.67(Bi _{1-x} La _x Fe _{0.97} Ga _{0.03} O ₃)-0.33(BaTiO ₃) where x=0.01(La1), x=0.03(La3), x=0.05(La5), and x=0.07(La7). | 136 |
| Figure 4.12 | Vogel Fulcher curve fitting for 0.67(Bi _{1-x} La _x Fe _{0.97} Ga _{0.03} O ₃)-0.33(BaTiO ₃) with compositions (a) x=0.01(La1), (b) x=0.03(La3), (c) x=0.05(La5), and (d) x=0.07(La7). | 138 |

| | | |
|--------------------|----------------------------------------------------------------------------------------------------------------------------------------------------------------------------------------------------------------------------------------------------------------------------------------------|-----|
| Figure 4.13 | Polarization vs Electric field and Current response hysteresis loops for $0.67(\text{Bi}_{1-x}\text{La}_x\text{Fe}_{0.97}\text{Ga}_{0.03}\text{O}_3)-0.33(\text{BaTiO}_3)$ where (a) $x=0.01(\text{La}1)$, (b) $x=0.03(\text{La}3)$, (c) $x=0.05(\text{La}5)$, (d) $x=0.07(\text{La}7)$. | 139 |
| Figure 4.14 | Leakage current plot for all compositions performed at an applied field of 30 kV/cm (b)PUND polarization profile for $0.67(\text{Bi}_{1-x}\text{La}_x\text{Fe}_{0.97}\text{Ga}_{0.03}\text{O}_3)-0.33(\text{BaTiO}_3)$ samples. | 141 |
| Figure 5.1 | The XRD patterns of various compositions for (a) BFSBT-x and (b) BLFBT-y ceramics. | 147 |
| Figure 5.2 | (a) UV-Vis diffuse reflectance spectroscopy (UV-Vis DRS) spectra of (a) BFSBT-x and (b) BLFBT-y where $x, y \leq 0.07$. | 149 |
| Figure 5.3 | Kubelka Munk Tauc plot for BFSBT-x with (a) $x=0.01$ (Sc1), (b) $x=0.03$ (Sc3), (c) $x=0.05$ (Sc5), and (d) $x=0.07$ (Sc7). | 151 |
| Figure 5.4: | Kubelka Munk Tauc plot for BLFBT with (a) $y=0.01$ (La1), (b) $y=0.03$ (La3), (c) $y=0.05$ (La5), and (d) $y=0.07$ (La7). | 152 |
| Figure 5.5 | Temperature dependent (a, c) dielectric constant plot for $x, y= 0.03, 0.07$ and (b, d) dielectric loss plot for $x, y=0.03$, respectively. | 155 |
| Figure 5.6 | Temperature dependent dielectric constant as a function of frequency for (a) $x=0.07$ (Sc7) and (b) $y=0.07$ (La7). | 155 |
| Figure 5.7 | Modified Curie–Weiss law linear fitting plot of $\ln(1/\epsilon_r - 1/\epsilon_m)$ vs $\ln(T - T_m)$ for (a) $x=0.07$ (Sc7) and (b) $y=0.07$ (La7) at 10 kHz. | 158 |
| Figure 5.8 | Vogel Fulcher model fitting for (a) $x =0.07$ (Sc7) in BSFT and (b) $y= 0.07$ (La7) in BLFT. | 158 |
| Figure 5.9 | Ferroelectric hysteresis loops for (a) $x, y=0.01$ (b) $x, y=0.03$ (c) $x, y=0.05$ and (d) $x, y=0.07$ in BFSBT-x and BLFBT-y. | 160 |
| Figure 5.10 | (a) P-E hysteresis loop depicting energy storage density calculation, and (b) Comparison of $W_{\text{Total}}, W_{\text{rec}}$ and η for different compositions of BFSBT-x and BLFBT-y. | 161 |

| | | |
|--------------------|-------------------------------------------------------------------------------------------------------------------------------------------------------------------------------|-----|
| Figure 6.1 | Powder XRD patterns at room temperature of pure BIT and Sm/Ta co-doped BIT at various sintering temperatures. | 170 |
| Figure 6.2 | Rietveld Refined patterns for (a) Pure BIT, (b) BITST S950, (c) BITST S1050 (d) BITST S1150 and (e) orthorhombic distortion and tetragonal strain variation with composition. | 171 |
| Figure 6.3 | FTIR spectra for Pure BIT, BITST S950, BITST 1050 and BITST S1150 measured in KBr mode. | 173 |
| Figure 6.4 | Full XPS spectrum of Pure BIT and BITST S1150. | 176 |
| Figure 6.5 | XPS spectra of O 1s for Pure BIT and BITST S1150. | 176 |
| Figure 6.6 | XPS spectra of Bi 4f for Pure BIT and BITST S1150. | 177 |
| Figure 6.7 | XPS spectra of Ti 2p for Pure BIT and BITST S1150. | 177 |
| Figure 6.8 | SEM micrographs of fractured surface for (a) Pure BIT, (b) BITST S950, (c) BITST S1050 and (d) BITST S1150. | 179 |
| Figure 6.9 | Average thickness of the platelet like microstructure of (a) Pure BIT, (b) BITST S950, (c) BITST S1050 and (d) BITST S1150. | 179 |
| Figure 6.10 | Elemental mapping and EDAX of (a,c)Pure BIT and (b,d) BITST S950. | 180 |
| Figure 6.11 | Polarization vs Electric field hysteresis loops for (a)Pure BIT, (b) BIT S950, (c) BIT S1050 and (d) BITST S1150. | 182 |
| Figure 6.12 | Comparison of PE loops at 10 Hz and 50 Hz for (a) Pure BIT, (b) BITST S950, (c) BITST S1050 and (d) BITST S1150. | 183 |
| Figure 6.13 | Current response loops for (a)Pure BIT, (b) BIT S950, (c) BIT S1050 and (d) BITST S1150 measured at 50Hz. | 186 |
| Figure 6.14 | Leakage current measurement for (a)Pure BIT, (b) BIT S950, (c) BIT S1050 and (d) BITST S1150 measured at 50kV/cm at 50Hz. | 188 |
| Figure 6.15 | PUND voltage profile and resulting output curve corresponding to pulse width and pulse delay of 10 ms for (a, c) pure BIT, (b, d) BITST S1150, respectively. | 189 |
| Figure 6.16 | PUND remnant polarization in four cycles for (a) Pure BIT and, (b) BITST S1150. | 191 |

| | | |
|--------------------|----------------------------------------------------------------------------------------------------------------------------------------------------------------------------------------------------------------------------------------|-----|
| Figure 6.17 | Temperature dependent (a) dielectric constant and (b) dielectric loss ($\tan \delta$) for BIT, BITST S950, BITST S1050, BITST S1150 measured at 10 kHz. | 193 |
| Figure 6.18 | Frequency dependent dielectric constant curves for BIT, BITST S950, BITST S1050, and BITST S1150 at 100 °C. | 194 |
| Figure 6.19 | Piezoelectric charge coefficient (d_{33}) for BIT, BITST S950, BITST S1050, and BITST S1150. | 196 |
| Figure 6.20 | Band gap calculation using Kubelka-Munk function Vs. Photon Energy plot for Pure BIT, BITST S950, BITST S1050 and BITST S1150 obtained from UV-vis diffuse reflection spectroscopy. | 199 |
| Figure 6.21 | (a) Excitation spectra and (b) Emission PL spectra for all the compositions. | 200 |
| Figure 6.22 | CIE color chromaticity diagram showing the wavelength and corresponding colour of emission wavelength (a) Pure BIT, (b) BITST S950, (c) BITST S1050, (d) BITST S1150 and (e) comparison showing effect of Sm, Ta incorporation in BIT. | 201 |

List of Tables

| Table No. | Captions | Page No. |
|------------------|-----------------------------------------------------------------------------------------------------------------------------------------------------------------------------------------------------------------------------------------------------------------------------------------------------------------------------------------------------------------|----------|
| Table 1.1 | Classification of crystallographic point groups using short Hermann-Mauguin Notation based on symmetry. | 9 |
| Table 1.2 | Summarizes the electrical properties of differently modified BF-BT systems. | 44 |
| Table 1.3 | Energy storage properties of some BF-BT and other lead free piezoceramics | 45 |
| Table 1.4 | Electrical characteristics of BNT-BT ceramics. | 49 |
| Table 1.5 | Electrical characteristics of BNKT ceramics after ion substitution | 49 |
| Table 2.1 | Precursors used for the synthesis of specific compositions. | 61 |
| Table 3.1 | Lattice parameters, space group, and refinement factors for all CS and AQ samples compositions. | 94-95 |
| Table 3.2 | Wavenumber, effective mass, frequency of vibration, force constant, and bond length of Fe-O bond for investigated Sc, Ga substituted BF-BT samples prepared by closed sintering (CS) and air quenching (AQ) methods. | 97 |
| Table 4.1 | Lattice parameters and refinement factors of $0.67(\text{Bi}_{1-x}\text{La}_x\text{Fe}_{0.97}\text{Ga}_{0.03}\text{O}_3)-0.33(\text{BaTiO}_3$ where $x=0.01(\text{La}1)$, $x=0.03(\text{La}3)$, $x=0.05(\text{La}5)$, and $x=0.07(\text{La}7)$ sintered at $980\text{ }^\circ\text{C}$ for 2 hours and annealed at $550\text{ }^\circ\text{C}$ for 12 hours. | 123 |
| Table 6.1 | Table for lattice parameters and refined parameters obtained from Rietveld refinement for Pure BIT and BITST sintered at $950\text{ }^\circ\text{C}$, $1050\text{ }^\circ\text{C}$ and $1150\text{ }^\circ\text{C}$. | 172 |
| Table 6.2 | Table 6.2 Piezoelectric charge constant and T_C values of different BIT based compounds. | 197 |

List of Symbols and Abbreviations

| | |
|-----------------|----------------------------------------------------------------------------------------|
| α | Absorption coefficient |
| λ | Wavelength |
| T_C | Curie temperature |
| $\tan\delta$ | Loss tangent (Dielectric loss) |
| ε' | Real part of the permittivity |
| ε'' | Imaginary part of the permittivity |
| d_{33} | Piezoelectric charge coefficient measured along poling direction |
| E | Electric field |
| E_a | Activation energy |
| E_c | Coercive field |
| E_g | Optical band gap |
| γ | Diffusivity constant |
| Ω | Resistance |
| θ | Theta (degrees) |
| χ^2 | Chi square (Goodness of Fit) |
| k_B | Boltzmann constant |
| T | Temperature |
| T_m | Transition Temperature at the maxima of temperature dependent dielectric constant plot |
| T_{VF} | Vogel Fulcher temperature |

| | |
|------------|--------------------------------------------------------------------------|
| τ | Relaxation time |
| VFT | Vogel Fulcher Tammann |
| XRD | X-ray Diffraction |
| FTIR | Fourier Transform Infrared |
| Vis | Visible light |
| UV | Ultraviolet radiation |
| DRS | Diffuse Reflectance Spectroscopy |
| SEM | Scanning Electron Microscope |
| EDS | Energy Dispersive X-ray Spectroscopy |
| XPS | X-ray Photoemission Spectroscopy |
| PUND | Positive Up Negative Down |
| PL | Photo Luminescence |
| MPB | Morphotropic Phase Boundary |
| FE | Ferroelectric |
| DC | Direct Current |
| PZT | Lead Zirconate, $\text{PbZr}_x\text{Ti}_{1-x}\text{O}_3$ |
| BFO | Bismuth Ferrite, BiFeO_3 |
| BT | Barium Titanate, BaTiO_3 |
| BF-BT | Bismuth Ferrite-Barium Titanate, BiFeO_3 - BaTiO_3 |
| KNN | Potassium Sodium Niobate, $\text{K}_{0.5}\text{Na}_{0.5}\text{NbO}_3$ |
| BNT | Bismuth Sodium Titanate, $\text{Bi}_{0.5}\text{Na}_{0.5}\text{TiO}_3$ |
| BIT | Bismuth Titanate, $\text{Bi}_4\text{Ti}_3\text{O}_{12}$ |
| PNR | Polar Nano Region |
| ϵ | Permittivity |

| | |
|-------|-------------------------|
| P_s | Saturated Polarization |
| P_r | Remnant Polarization |
| E_c | Coercive Electric Field |